Received: 4 September 2021 | Revised: 9 January 2022 | Accepted: 10 January 2022

DOI: 10.1111/ffe.13658

ORIGINAL ARTICLE

FFEMS Fatigue & Fracture of Engineering Materials & Structures WILEY

Quantitative thermographic method for fatigue life prediction under variable amplitude loading

Ensheng Feng[1] | **Xiaogang Wang**[1] | **Chao Jiang**[1] | **Vincenzo Crupi**[2]

[1]State Key Laboratory of Advanced Design and Manufacturing for Vehicle Body, College of Mechanical and Vehicle Engineering, Hunan University, Changsha, China

[2]Department of Engineering, University of Messina, Messina, Italy

Correspondence
Xiaogang Wang, State Key Laboratory of Advanced Design and Manufacturing for Vehicle Body, College of Mechanical and Vehicle Engineering, Hunan University, 410082 Changsha, China.
Email: xgwang@hnu.edu.cn
Vincenzo Crupi, Department of Engineering, University of Messina, Contrada di Dio, Sant'Agata, 98166. Messina, Italy.
Email: crupi.vincenzo@unime.it

Funding information
National Defence Fundamental Research Foundation of China, Grant/Award Number: JCKY2020110C105; Special Funds for the Construction of Innovative Provinces in Hunan Province, Grant/Award Number: 2019GK4006; National Science Fund for Distinguished Young Scholars, Grant/Award Number: 51725502; National Natural Science Foundation of China, Grant/Award Number: 51975195

Abstract

Quantitative thermographic methodology (QTM), which takes energy dissipation as a fatigue indicator, has been successfully applied to predict the fatigue life of materials and welded joints under constant amplitude loading. This study advances the QTM approach for predicting the fatigue life under variable amplitude loading in both low and high cycle fatigue regimes. Experimental data, obtained by fatigue tests under variable amplitude loading, were used in order to apply the developed QTM approach and to demonstrate that it is able to take into account the loading sequence effect. Good predictions of the fatigue life were achieved.

KEYWORDS

energy dissipation, fatigue, S-N curve, thermographic method, variable amplitude loading

1 | INTRODUCTION

A variety of approaches for fatigue strength and life assessment of metallic materials and welded joints have been developed and reported in the literature. The most common approaches include notch stress intensity factor (N-SIF) approach,[1–3] averaged strain energy density (SED) approach,[4–6] critical distance methods (CDMs),[7–9] notch strain approach,[10] structural strain approach,[11–13] crack propagation approach,[14] and thermal methods,[15–29] which are based on the self-heating effect of a metallic specimen subjected to fatigue loading. It is known that the fatigue failure of metallic materials is caused by cyclic plasticity, which produces heat dissipation and

temperature increment.[24,29–32] Based on this self-heating mechanism, the thermal methods can be broadly classified into the following categories:

a. the thermal methods that adopt the temperature directly measured on the surface of the specimen as the fatigue indicator[15–23];
b. the thermal methods processing the thermal signal in order to assess its components[24–26];
c. the thermal methods based on entropy considerations derived from surface temperature measurements[27];
d. the thermal methods using the specific heat loss.[28,29]

The thermographic method (TM)[17] is based on the assumption that the fatigue strength can be evaluated as the highest stress level that produces no temperature increment on the surface of a specimen subjected to fatigue loading. It allows a reliable and rapid prediction of the fatigue strength[17] and the S-N curve[18] by applying a very limited number of fatigue tests. At present, most of the TMs are limited to high cycle fatigue (HCF) conditions, and only a few are applicable to low cycle fatigue (LCF) conditions, which occur during the service life of certain structures. The TM was applied for the first time to the LCF regime by Crupi et al.[33]

A new concept of quantitative thermographic methodology (QTM) was initially proposed by some of the authors in the work.[34] This new method was successfully applied to smooth and notched (with artificial holes) A36 mild steel specimens and butt welded AH36 steel joints.[35] It was further developed in Wang et al[36] by using energy dissipation instead of temperature increment as the fatigue indicator. The temperature increment is directly related to the heat dissipation from the strain energy, but it also depends on the heat exchange conditions with the environment.[37] Typically, the temperature manifests a three-stage evolution trend during the fatigue process. In the initial Stage I, the accumulated plastic deformation at the beginning of the test can cause a rapid temperature growth. This temperature growth will be limited by the heat lost due to the heat exchange between the specimen and the surrounding environment. When the heat lost is equal to the net heat produced by the plastic deformation, the temperature will reach a steady state, namely, Stage II.[17–21,25,38–40] In most metallic materials, Stage II will be predominant in the fatigue lifespan. In the final Stage III, the temperature suddenly rises due to macroscopic fatigue cracking, which is a sign of fatigue failure.

The temperature reaches the thermal steady state because the dissipated energy and the heat loss caused by the heat exchange between the sample and the environment have reached equilibrium. Affected by the heat exchange conditions, the temperature evolution of the specimen surface may not have a stable stage. In addition, even if the heat exchange conditions are unchanged, there will be cases where the temperature rises significantly without a stable phase. This situation is usually caused by unstable generation of dissipated energy when the load level is high. De Finis et al[25] studied this atypical behavior and proposed three thermal indexes (the slope of the first temperature data series, the mean value of the same series, and the maximum temperature reached in the loading step) to replace the stable state temperature to estimate the fatigue limit. De Finis et al[25] concluded that when there is no steady-state temperature, these three thermal indicators can also be successfully used to predict the fatigue limit and the slope of the first temperature has the best prediction accuracy. Similarly, the dissipated energy under these temperatures can also be used to evaluate the fatigue behavior under unsteady-state conditions.

Here, it can be noted that the variation of the apparent temperature is controlled by the energy dissipation mechanism of the material behind. Indeed, the fatigue damage phenomenon is an energy dissipation process. The dissipated energy can be regarded as an intrinsic indicator of fatigue damage, which can be sensitively detected by thermographic technique. Based on this understanding, the improved QTM is based on the assumption that, when the dissipated energy accumulation in the material reaches a critical value, that is, the energy tolerance of the material (denoted by E_C), fatigue failure occurs.

The fatigue assessment becomes more complex in the presence of a multiaxial stress state, and several approaches based on the critical plane have been developed in the literature.[41–43] Thus, the QTM was, recently, successfully extended to some more complicated fatigue conditions, such as multiaxial fatigue[44] and fatigue crack propagation[45] and provided reliable fatigue life predictions.

Although QTM has made significant progress in recent years, there are still some challenges on its path to real engineering applications. One of the key issues is the variable amplitude loading (VAL) that occurs in most engineering structures and causes fatigue failure. The current design codes and standards generally recommend the Palmgren–Miner rule (commonly referred to as Miner's rule),[46,47] which represents a linear fatigue damage model for predicting the residual life of structures under VAL, because of its simplicity and ease of application. For instance, Meneghetti et al[48] successfully developed an energy-based fatigue life prediction model based on Miner's rule and applied it to VAL fatigue. Nevertheless, there is a major shortcoming of Miner's rule: It cannot consider the loading sequence effect, which may affect the fatigue life for the following effects: stress

intensification effect, damage interaction effect, damage sequence effect, and crack opening effect.[49] The state of the art of cumulative fatigue damage and life prediction theories[50–55] were reviewed by Fatemi and Yang[56] and by Jinescu.[57] More than 60 fatigue models[57] have been proposed in order to overcome this limitation, but they require either the determination of some material parameters, which are not easy to evaluate, or modifications to the S-N curve of the material. Therefore, the fatigue life prediction under VAL remains an open issue.

The objective of this study is to develop QTM approach for predicting the fatigue life under VAL in both LCF and HCF regimes. Experimental data, obtained by fatigue tests under VAL, were used to explore the ability of the developed QTM approach to deal with variable amplitude fatigue and to demonstrate that it is able to take into account the loading sequence effect. The fatigue tests involve three variable amplitude load spectra of two-step loading, repeating two-step loading, and periodical overloading.

The proposed QTM approach is an energy-based approach for variable amplitude fatigue life prediction, which uses thermography to estimate some pertinent thermal parameters (E_d and E_C). The proposed approach is still called QTM in order to maintain consistency and continuity with previous studies.

2 | METHODOLOGY

The fatigue life model based on the QTM for constant amplitude fatigue has been well established, which can be referred to previous works of the authors.[36,44] In this work, before elucidating the developed model based on the energy dissipation evaluation for VAL life prediction, a brief introduction to QTM is given within the thermodynamic framework.

The time-dependent temperature response of an elastic–plastic, isotropic, homogenous material subjected to cyclic loading may be expressed using the first law of thermodynamics:

$$\dot{U} = \dot{W} - \dot{Q} \tag{1}$$

where $\dot{U}$ is the rate of internal energy accumulation in the material, $\dot{Q}$ is the rate of energy dissipated as heat, and $\dot{W}$ is the rate of mechanical work applied to the material.

Based on the first law of thermodynamics, Chrysochoos and other researchers[37,58,59] proposed the following form of the heat diffusion equation to determine the heat sources from the temperature variation within the thermodynamic framework:

$$\rho C \frac{\partial \theta}{\partial t} - k\Delta\theta = s_{the} + d_1 + r \tag{2}$$

where ρ represents the mass density, C the specific heat, k the isotropic thermal conductivity, t the current time, and Δ the Laplace operator.

The terms involved in the above equation have the following physical significance:

- $\rho C\dot{\theta}$ is the energy release rate due to temperature increase.
- $-k\Delta\theta$ is the heat rate loss by conduction.
- S_{the} is the thermoelastic term, which is generally neglected in the heat source estimation.
- d_1 is the intrinsic dissipation, which is the difference between the rate of mechanical work $\dot{W}$, the elastic energy variation rate $\dot{U}_e$, and the internal energy storage rate $\dot{U}_D$ due to material damage.
- r is the external volume heat supply, which is due to the heat exchange with the surrounding environment.

The external heat source r characterizes the heat exchange between the specimen and the environment. For the fatigue test conducted at room temperature, it represents actually the heat loss into the environment. The accurate evaluation of the heat loss Q is a challenging issue,[58] because it can operate in multiple ways through conduction, convection, and radiation. These elements are difficult to be accurately estimated as they strongly depend on the boundary conditions of the specimen and environmental factors.

Fatigue is manifested as an irreversible microstructure evolution, which causes the accumulation of stored energy in the material. Therefore, a portion of the plastic energy (i.e., U_D) is directly related to fatigue damage, but it is not easy to measure this stored energy directly, so the dissipated energy d_1 is usually measured to indirectly evaluate the internal stored energy U_D due to material damage. The plastic energy in the fatigue process is partially converted into stored energy, but the majority of it is dissipated as heat. Some studies[60–64] have shown that for most metallic materials, the proportion of dissipated plastic energy, namely, β, is above 80%. The parameter β is therefore commonly assumed as a material constant, and for most metals $\beta \approx 0.9$,[60] such as low-carbon steel Q235,[61] medium-carbon steel SAE1045,[62] aluminum alloy,[63] and pure copper.[64]

Generally, a simple solution can be adopted by presuming a linear relationship between the heat loss and temperature variation[37,59,64]:

$$r = -\rho C \frac{\theta}{\tau} \tag{3}$$

where τ is a time constant characterizing local heat losses and can be estimated using the stage of thermal return to equilibrium after the fatigue test.

Thus, by taking into account the above estimations of S_{the} and r, the heat diffusion equation can be further simplified by removing the Laplacian term:

$$\rho C\left(\frac{\partial\theta}{\partial t}+\frac{\theta}{\tau}\right)=d_1 \tag{4}$$

The QTM approach considers the stabilized Stage II of the specimen subjected to fatigue loading (described above in Section 1) as an asymptotic temperature increment stage where $\theta=\theta_{AS}$, then the temperature variation rate $\frac{\partial\theta}{\partial t}$ equals zero at this stage, and then an asymptotic (or stabilized) intrinsic dissipation $d_{1,AS}$ can be obtained by

$$\rho C\frac{\theta_{AS}}{\tau}=d_{1,AS} \tag{5}$$

Equation 5 shows that the stabilized dissipation $d_{1,AS}$ depends not only on the temperature θ_{AS} but also on the heat exchange condition characterized by a time constant τ. It is thus interesting to adopt the energy term $d_{1,AS}$ instead of temperature θ_{AS} for the quantification of the fatigue damage level.

For the sake of convenience, the dissipation per cycle d_1/f ($f=N/t$) is adopted instead of d_1 the dissipation per second, so the dissipated energy per cycle E_d is defined as

$$E_d=d_{1,cycle}=\frac{d_{1,AS}}{f}=\rho C\frac{\theta_{AS}}{f\tau} \tag{6}$$

The dissipated energy per cycle E_d depends on the fatigue damage and is, therefore, regarded as the fatigue indicator. E_d can be evaluated by the asymptotic temperature θ_{AS} of the specimen surface, which can be detected by the thermographic technique.

Because the dissipated energy is considered as fatigue indicator, it is necessary to define a relevant energy tolerance concept[34] for the purpose of fatigue life evaluation by QTM. Here, it is considered that the cumulated energy dissipation can be used to characterize such an energy tolerance. The total cumulated dissipation during the fatigue process can be obtained through the integral of d_1 over the number of cycles to failure N_f.

The total cumulated energy dissipation $d_{1,\mathrm{cum}}$ is considered as a material parameter that characterizes the energy tolerance to failure for a given material under cyclic loading, so it is equivalent to the energy tolerance to failure E_C:

$$E_C=d_{1,cum}=\int_0^{N_f}\frac{d_1}{f}dN \tag{7}$$

Because the stabilized Stage II is predominant in the fatigue lifespan as shown in Figure 1, the number of cycles to failure N_f can be then assumed equal to the span of Stage II ΔN_{AS} ($=N_{AS,f}-N_{AS,0}$). Thus, by considering only the stabilized stage (to represent the whole fatigue process) and adopting Equation 7, the energy tolerance to failure E_C[36] can be estimated through

$$E_C=\int_0^{N_f}\frac{d_{1,AS}}{f}dN=\frac{\rho C}{f\tau}\theta_{AS}N_f \tag{8}$$

Then, according to the dissipated energy per cycle E_d defined by Equation 6, one can obtain

$$E_C=E_d\cdot N_f \tag{9}$$

Thus, the QTM defines fatigue damage based on the linear accumulation of energy, that is, fatigue failure occurs when the accumulated energy reaches the energy tolerance E_C.

A flow diagram of the fatigue testing procedure based on QTM is shown in Figure 1. A stepwise amplitude-increasing fatigue loading procedure is applied to the specimen block by block,[65,66] and the temperature of the specimen surface is measured simultaneously using an infrared camera. In each loading block, fatigue loading is not suspended until the stabilized Stage II is reached, which usually requires thousands of cycles for steels.[62,65,66] Then, the asymptotic temperature θ_{AS} of Stage II used for fatigue damage evaluation can be assessed. It is important to note that the thermal images need to be smoothed in order to remove the thermal noises and increase the signal-to-noise ratio. In most cases, Gaussian filtering can achieve a satisfactory result.[58] According to the QTM, the intrinsic dissipation E_d can be evaluated according to Equation 6 by taking into account the heat exchange with the surrounding environment at Stage II.[36,44,58] And the energy tolerance E_C can be evaluated by Equation 8 or 9 by integrating the total energy dissipation until the fatigue failure of the specimen.[65]

The previous studies[36,44] have demonstrated that the energy tolerance E_C depends not only on material properties but also on the fatigue mechanism of the material. Thus, it is reasonable to assume that the energy tolerance of the material in the LCF regime is different from that in the HCF regime. In other words, two different E_C can be defined, that is, $E_{C,LCF}$ representing the E_C in the LCF regime and $E_{C,HCF}$ representing the E_C in the HCF regime. In order to distinguish the LCF regime and HCF

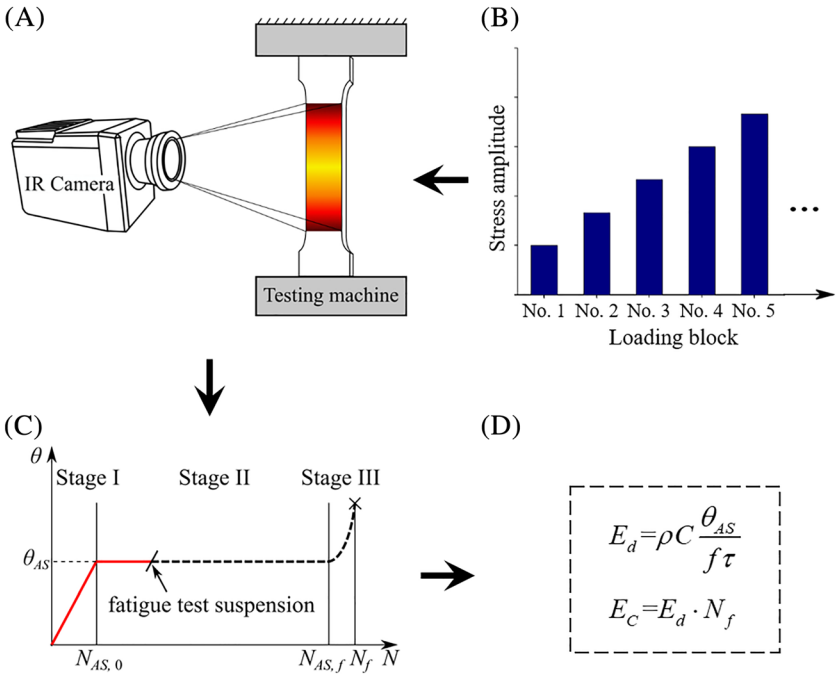

FIGURE 1 A flow diagram of the fatigue testing procedure based on QTM: (A) experimental setup; (B) stepwise loading procedure; (C) average temperature evolution; (D) evaluation of the intrinsic dissipation E_d and energy tolerance E_C [Colour figure can be viewed at wileyonlinelibrary.com]

regime in the S-N curve, the concept of transition life N_t can be introduced to represent the fatigue life boundary between the two fatigue regimes LCF and HCF. The transition life N_t generally corresponds to a certain applied strain amplitude ε_{at}, which can be used to distinguish between LCF and HCF. When the applied strain amplitude is higher than ε_{at}, it corresponds to the LCF regime, in which case $E_{C,LCF}$ applies. But when the applied strain amplitude is lower than or equal to ε_{at}, it corresponds to the HCF regime, in which case $E_{C,HCF}$ applies Then, according to the QTM, the $E_{C,LCF}$ and $E_{C,HCF}$ can be estimated, respectively, by

$$E_{C,LCF} = E_d \cdot N_f, \text{for } \varepsilon_a > \varepsilon_{at} \tag{10}$$

$$E_{C,HCF} = E_d \cdot N_f, \text{for } \varepsilon_a \le \varepsilon_{at} \tag{11}$$

Here, it is worth noting that the above definition of $E_{C,LCF}$ and $E_{C,HCF}$ is a simplification of a complex fatigue phenomenon. In practical applications, whether to choose $E_{C,LCF}$ or $E_{C,HCF}$ can be determined by the specific applied strain amplitude of a given loading spectrum, which may contain both LCF-level and HCF-level load components. In the following model construction, a unified E_C is used for the simplicity of expression.

The conventional QTM treats VAL by using an energy form of Miner's rule,[34,48] which cannot consider nonlinear damage accumulation and loading sequence effects. In this study, a new QTM-based model has been developed to take into account these effects, which uses an exponential form to describe nonlinear fatigue damage evolution. Considering a load spectrum composed of multiple block loads with different stress (or strain) amplitudes, the cumulative fatigue damage of the loaded material at a given time in its service life can be expressed by

$$D_i = 1 - \left[1 - \frac{(n_{i-1,e} + \Delta n_i) \cdot E_{d,i}}{E_C}\right]^{q_i} \tag{12}$$

where D_i represents the cumulative fatigue damage at the end of the ith block load, $E_{d,i}$ represents the dissipated energy per cycle under the ith block load, n_i represents the cumulative number of cycles at the end of the ith block load, Δn_i represents the number of cycles of the ith block load, $n_{i-1,e}$ represents the equivalent number of cycles of n_{i-1} corresponding to the ith block load, and q_i represents the exponent of the nonlinear model.

The above equation shows that the cumulative fatigue damage D_i can be composed into two parts. The first part is the damage accumulated in the previous $(i-1)$ blocks, that is, from the first block to the $(i-1)$th block. This part is dependent on the parameter $n_{i-1,e}$ that represents the equivalent number of cycles of n_{i-1} corresponding to the ith block load under the principle of equivalent transformation of fatigue damage. Then, it can be determined by $n_{i-1,e}$ in combination with the damage level of the ith block load characterized by the thermal parameter $E_{d,i}$. The second part of the cumulative fatigue damage is the damage accumulated in the ith block. This part can be determined directly by Δn_i and $E_{d,i}$.

It can also be noted that the proposed model adopts an exponential form, which is commonly used to describe

the evolution of nonlinear fatigue damage.[67–69] The difference is that it uses dissipated energy to quantify fatigue damage instead of directly using the number of cycles. The advantage is that it only requires a few stepwise loading tests to efficiently acquire the relevant parameters (i.e., E_C and E_d) instead of extensive time-consuming fatigue tests to obtain a complete S-N curve.

The exponential term of the nonlinear model q_i is defined as

$$q_i = \frac{\delta_i}{\mu_i} \tag{13}$$

where the parameter δ_i describes the nonlinearity of fatigue damage accumulation in terms of dissipated energy. It can be expressed by

$$\delta_i = \frac{3}{2\left(\ln\frac{E_C}{E_{d,i}} - 1\right)} \tag{14}$$

This formula is inspired by the original definition of δ_i by Aeran et al,[68] which defines δ_i as a nonlinear function of fatigue life, that is, $\delta = -1.25/\ln N_f$. In this work, the parameter δ_i depends only on the two thermal parameters of E_C and $E_{d,i}$, without involving other material parameters.

In order to further consider the effect of the loading sequence, another parameter μ_i is added to the exponential term. It describes the influence of the interaction of two adjacent blocks with different load levels on fatigue damage evolution, which is defined as

$$\mu_i = \left(\frac{E_{d,i-1}}{E_{d,i}}\right)^{\frac{1}{4}} (i \geq 2) \tag{15}$$

It can be noted from the above equation that the parameter μ_i represents the influence of the previous $(i-1)$th block load on the current ith block load. This definition is also a variant of the original definition of μ_i by Aeran et al,[68] where μ_i is defined as the function of the ratio of two adjacent load levels, namely, $\mu_i = (\sigma_{i\text{-}1}/\sigma_i)^2$. Here, the influence parameter μ_i is quantified using the dissipated energy evaluated under two adjacent load levels, i.e., $E_{d,i-1}$ and $E_{d,i}$. The exponential term in Equation 15 is a measure of the intensity of the interaction between the two adjacent block loads. It is usually considered as an empirical parameter. Here this parameter is set to 1/4 because this investigation has shown that this value is suitable for the proposed QTM approach. Here, it is worth noting that for the first block load without previous load history, μ_i is equal to 1 (i.e., no interaction).

Then, Equation 12 can be rewritten as the following form with the expansion expression of the parameter q_i.

$$D_i = 1 - \left[1 - \frac{(n_{i-1,e} + \Delta n_i)\cdot E_{d,i}}{E_C}\right]^{\frac{\delta_i}{\mu_i}} \tag{16}$$

Another key parameter in the proposed model is $n_{i-1,e}$ that represents the equivalent number of cycles of n_{i-1} corresponding to the ith block load. The assessment of $n_{i-1,e}$ depends on the knowledge of the previous cumulative damage D_{i-1} before the current ith block load. And these two parameters can be correlated by

$$1 - \left(1 - \frac{n_{i-1,e}\cdot E_{d,i}}{E_C}\right)^{q_i} = D_{i-1} \tag{17}$$

Equation 17 is based on a concept of equivalent transformation of fatigue damage, which assumes that the fatigue damage accumulated in the previous blocks (i.e., from the first block to the $(i-1)$th block) can be equivalently transformed to the current block (i.e., the ith block). This equivalent transformation adopts an energy form. The invariable is the energy dissipation level $E_{d,i}$ under the ith block load, and the variable is the equivalent number of cycles $n_{i-1,e}$, which needs to be estimated to satisfy this transformation. Then, Equation 17 can be further rewritten as the following form for the assessment of $n_{i-1,e}$.

$$n_{i-1,e} = \left[1 - (1 - D_{i-1})^{\frac{1}{q_i}}\right] \cdot \frac{E_c}{E_{d,i}} \tag{18}$$

One can note that a significant feature of the proposed method is that the assessment of the current cumulative damage (at the ith block) requires knowledge of the previous cumulative damage (before the ith block). The latter is also a prerequisite for resolving the equivalent number of cycles $n_{i-1,e}$ according to the above equation. A special case is the assessment of the cumulative fatigue damage of the first block D_1, where there is no previous loading. Then, Equation 16 cannot be applied directly. In fact, this can be considered as a special case of Equation 16, where the first part presenting damage accumulated in the previous block can be canceled and then D_1 can be expressed as

$$D_1 = 1 - \left[1 - \frac{\Delta n_1 \cdot E_{d,1}}{E_C}\right]^{\delta_1} \tag{19}$$

After obtaining D_1, the $n_{i-1,e}$ of the second block load, that is, $n_{1,e}$, can be calculated using Equation 18. And

then this parameter can be used for the estimation of D_2 according to Equation 16. By following this procedure, the D_i for a given VAL spectrum can be assessed through Equations 16 and 18.

The last important issue is the criterion of fatigue failure. In this work, the critical condition for fatigue failure is defined as

$$D_i = 1 \tag{20}$$

This is the same as the conventional Miner's rule to keep the model as simple as possible. Figure 2 shows the flow chart of the developed model for fatigue analysis under VAL. It can be used to evaluate fatigue damage D_i and determine whether fatigue failure occurs for a given VAL spectrum. Then, the total fatigue life N_f at $D_i = 1$ can be evaluated.

Another important application of the proposed model is the residual fatigue life prediction. Considering a specimen subjected to a VAL spectrum composed of multiple blocks, it is assumed that fatigue failure will occur under the ith block load and Δn_i is an unknown to predict, that is, the so-called residual fatigue life (denoted by N_r). In this case, by substituting Equation 20 into Equation 16, the residual fatigue life can be obtained by

$$N_r = \Delta n_i = \frac{E_C}{E_{d,i}} - n_{i-1,e} \tag{21}$$

Then, the residual fatigue life N_r can be predicted by Equation 21.

3 | MODEL APPLICATION

The first preliminary experimental campaign to apply the proposed model was carried out using the experimental data extracted from reference.[49] It contained different types of VAL fatigue tests applied to a 316 stainless steel, namely, two-step loading, repeating two-step loading, and periodical overloading tests, which are summarized in Table 1. All these fatigue tests were performed in strain-controlled mode, and the loading ratio R was -1. Figure 3 shows the ε_a–N_f curve of the test material

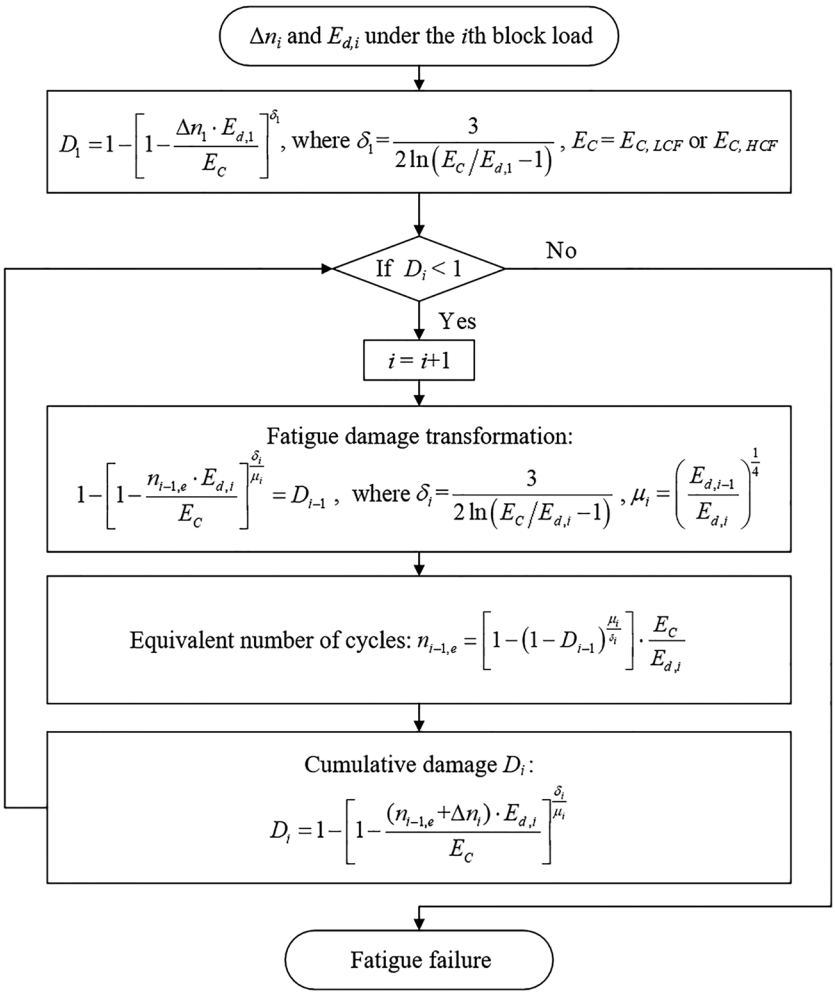

FIGURE 2 Flow chart of the developed QTM-based nonlinear fatigue model to deal with variable amplitude loading spectrum

TABLE 1 Summary of the VAL fatigue tests[49]

	Case 1	Case 2	Case 3
Type of test	Two-step loading	Repeating two-step loading	Periodical overloading
Number of tests	10	5	4

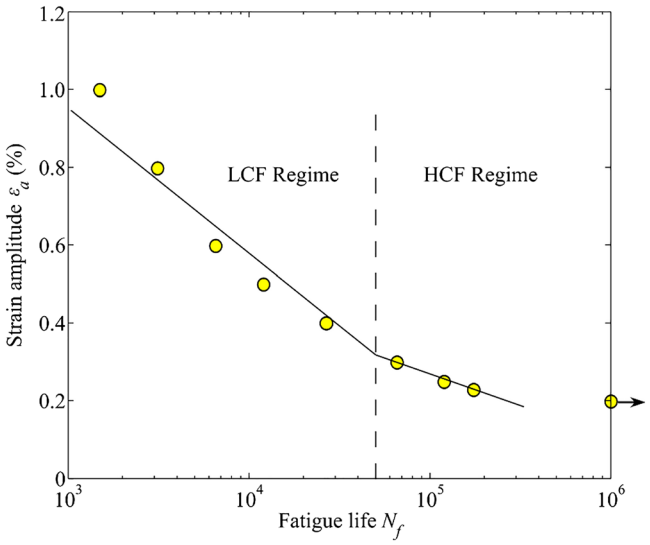

FIGURE 3 ε_a–N_f curve of the test 316 stainless steel reproduced from reference[49] [Colour figure can be viewed at wileyonlinelibrary.com]

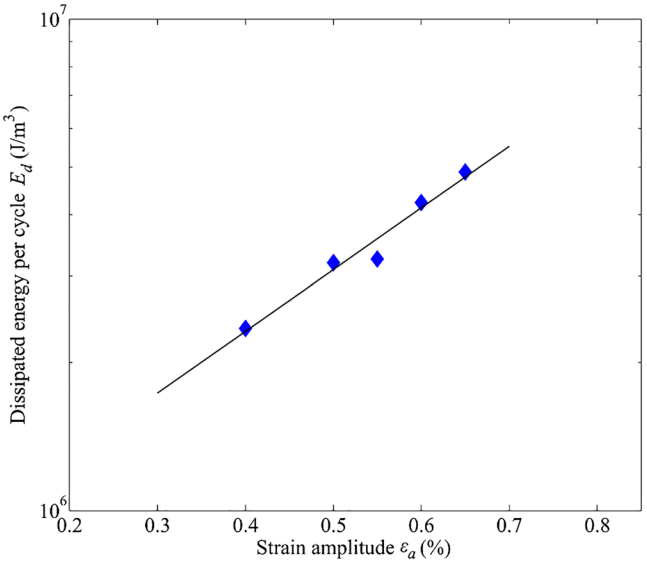

FIGURE 4 E_d–ε_a curve of a 316L steel obtained using experimental data reported in the work[44] [Colour figure can be viewed at wileyonlinelibrary.com]

obtained under constant amplitude fatigue tests. In this diagram, the LCF regime and the HCF regime can be separated by the transition life N_t, which can be estimated to be about 50,000 cycles for the present material. Its corresponding strain amplitude ε_{at} is about 0.32%. This value can be used to distinguish between the LCF regime and the HCF regime.

In previous work of the authors,[44] the energy dissipation behavior of a 316L stainless steel, which is very similar to the present 316 stainless steel,[49] has been investigated. It allows the establishment of an E_d–ε_a relationship as below.

$$\log(E_d) = 1.26\varepsilon_a + 5.86 \tag{22}$$

The E_d–ε_a relationship established above is shown in Figure 4. It was applied to the fatigue analysis of this work in view of the high similarity of fatigue properties between the 316 steel and the 316L steel, as shown in the literature.[70–72] It is also assumed here that the established E_d–ε_a relationship has general applicability to a wider range of strain amplitudes, which is able to cover the fatigue data reported in Figure 3. Then, for all the constant amplitude fatigue test data shown in Figure 3, their corresponding intrinsic dissipation E_d can be estimated. Based on the obtained data of E_d and N_f, the two energy tolerances $E_{C,LCF}$ and $E_{C,HCF}$ can be estimated in each fatigue regime through Equations 10 and 11, respectively. It provided an estimated $E_{C,LCF}$ of 2.66×10^{10} J/m^3 and $E_{C,HCF}$ of 1.72×10^{11} J/m^3 as the average value for each fatigue regime.

The proposed fatigue model was verified under three different VAL conditions, namely, two-step loading (Case 1), repeating two-step loading (Case 2), and periodical overloading (Case 3). The prediction results of the model in the three cases and its comparison with experimental data are presented below.

3.1 | Case 1 of two-step loading

The first case focuses on a two-step loading spectrum composed of two block loads with different strain amplitudes, as schematically shown in Figure 5. According to this loading spectrum, 10 fatigue tests were carried out.[49] The specific loading conditions and part of the experimental data are reported in Table 2. The 10 fatigue tests can be divided into two groups. The first group involves a

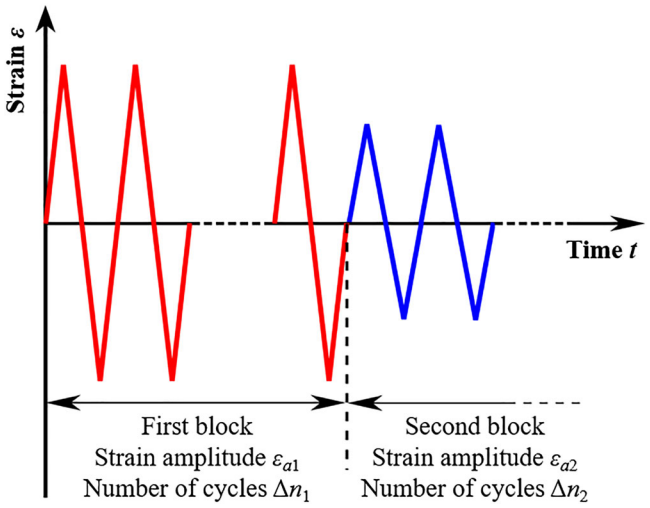

FIGURE 5 Schematic presentation of two-step loading spectrum of Case 1 [Colour figure can be viewed at wileyonlinelibrary.com]

TABLE 2 Loading conditions and part of the experimental data of fatigue tests in Case 1[49]

Test no.	Loading type	First step ε_{a1} (%)	First step Δn_1	Second step ε_{a2} (%)
1	H-L	1.0	750	0.5
2	H-L	1.0	750	0.3
3	H-L	1.0	750	0.3
4	H-L	0.5	6000	0.3
5	H-L	0.5	6000	0.25
6	H-L	0.5	6000	0.2
7	L-H	0.5	6000	1.0
8	L-H	0.3	32,000	1.0
9	L-H	0.3	32,000	0.5
10	L-H	0.25	59,001	1.0

high load followed by a low load (Type H-L), and the second group is the opposite, which involves a low load followed by a high load (Type L-H). The purpose of using these different loading combinations is to test the applicability of the proposed model to any two-step VAL. The service life of the material under the first block load (i.e., the number of cycles Δn_1) has been given in Table 2, and now what needs to be predicted is the residual fatigue life N_r under the second block load (i.e., the number of cycles Δn_2).

The prediction results by the proposed model are reported in Table 3, where $N_{r,p}$ represents the predicted residual life and N_r represents the experimental data of the residual life Δn_2. Their comparison is illustrated in Figure 6. The solid line represents the ideal prediction with $N_{r,p}$ equal to N_r in the lifespan involved, and the dashed lines represent the scatter band of fatigue life with an error factor of 2. The majority of the data points fall within the specified scatter band, confirming that there is a good agreement between the predicted residual lives and the experimental results.

TABLE 3 Predicted residual life and comparison with experimental data in Case 1

Test no.	Loading type	$N_{r,p}$	N_r
1	H-L	3837	6414
2	H-L	29,376	15,712
3	H-L	29,376	20,000
4	H-L	16,437	33,688
5	H-L	17,328	34,000
6	H-L	18,188	91,500
7	L-H	1025	1215
8	L-H	1749	1164
9	L-H	6648	8368
10	L-H	1562	1598

The prediction accuracy of the proposed model can be quantified by introducing an error factor E_S, which represents the standard deviation of the predicted results from the experimental data. It can be defined as[73]

$$E_S = \sqrt{\frac{\sum_{i=1}^{n} \left[\lg(N_{f,p}) - \lg(N_f)\right]^2}{n}} \tag{23}$$

The calculated error factor E_S of the proposed model is about 0.296. This value is lower than the E_S given by using the classic Miner's rule (based on the ε_a–N_f curve of the test material), which is about 0.308. Here, it should be emphasized that this comparison is made under a very simple VAL condition, which involves only two block loads. In this case, Miner's rule can generally provide satisfactory predictions, because both the nonlinear damage accumulation effect and the loading sequence effect are not significant. Hence, the applicability of the proposed model to more complex VAL conditions needs to be further tested and compared with Miner's rule. They are Case 2 and Case 3 presented below.

3.2 | Case 2 of repeating two-step loading

The second case is concerned with a repeating two-step loading spectrum. It is composed of two block loads with

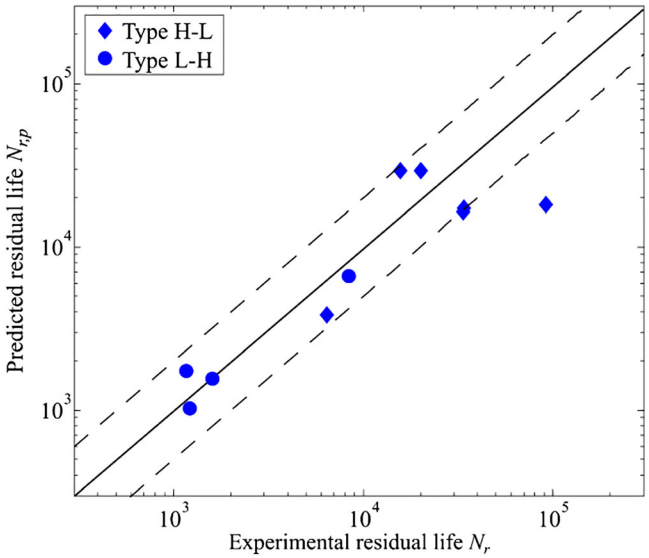

FIGURE 6 Comparison between the predicted residual life and the experimental data in Case 1 [Colour figure can be viewed at wileyonlinelibrary.com]

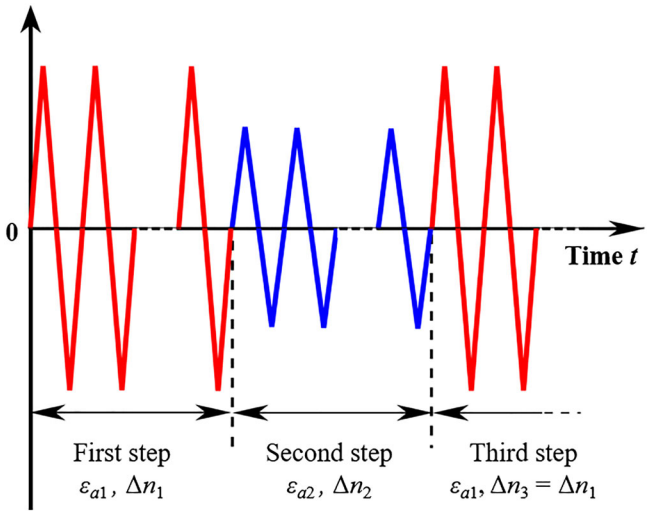

FIGURE 7 Schematic presentation of repeating two-step loading spectrum of Case 2 [Colour figure can be viewed at wileyonlinelibrary.com]

different strain amplitudes that are repeatedly applied during the fatigue test until failure occurs, as schematically shown in Figure 7. In this case, five fatigue tests were conducted,[49] and their loading conditions and part of the experimental data are shown in Table 4. The reported experimental data only contain the applied number of cycles of the first and second steps, that is, Δn_1 and Δn_2. Their sum $(\Delta n_1 + \Delta n_2)$ usually only accounts for a small portion of the total fatigue life. Hence, the prediction herein is for the total fatigue life N_f under the repeating two-step loading spectrum.

TABLE 4 Loading conditions and part of the experimental data of fatigue tests in Case 2[49]

	First step		Second step	
Test no.	ε_{a1} (%)	Δn_1	ε_{a2} (%)	Δn_2
1	1.0	75	0.3	3200
2	0.5	600	0.3	3200
3	0.5	60	0.3	320
4	0.5	600	0.2	29,000
5	0.5	60	0.2	2900

TABLE 5 Predicted fatigue life and comparison with experimental data in Case 2

Test no.	$N_{f,p}$	N_f
1	31,526	22,991
2	34,343	38,400
3	34,772	33,415
4	92,487	175,550
5	96,014	131,301

The predictions by the proposed model are reported in Table 5, where $N_{f,p}$ represents the predicted fatigue life and N_f represents the experimental fatigue life. Their comparison is shown in Figure 8. The dashed lines represent the scatter band of fatigue life with an error factor of 2. It exhibits that all the data points fall within the scatter band. Thus, it demonstrates that satisfactory predictions of the fatigue life for Case 2 are achieved by using the proposed model. The error factor E_S is estimated to be about 0.153, which is significantly lower the value 0.255 given by Miner's rule based on the ε_a–N_f curve. Hence, it shows that the proposed model has better applicability to the life prediction under VAL than Miner's rule.

3.3 | Case 3 of periodical overloading

The third case is focused on a periodical overloading spectrum. In this case, an overload is applied periodically during the fatigue test, as schematically shown in Figure 9. Fatigue tests were performed under four different loading conditions,[49] as reported in Table 6. The total fatigue life N_f is expected to be predicted.

The predictions by the proposed model and the experimental results are reported in Table 7, and their comparison is shown in Figure 10. The dashed lines in the figure represent the scatter band of fatigue life with an error factor of 2. It shows that three out of all four data points fall

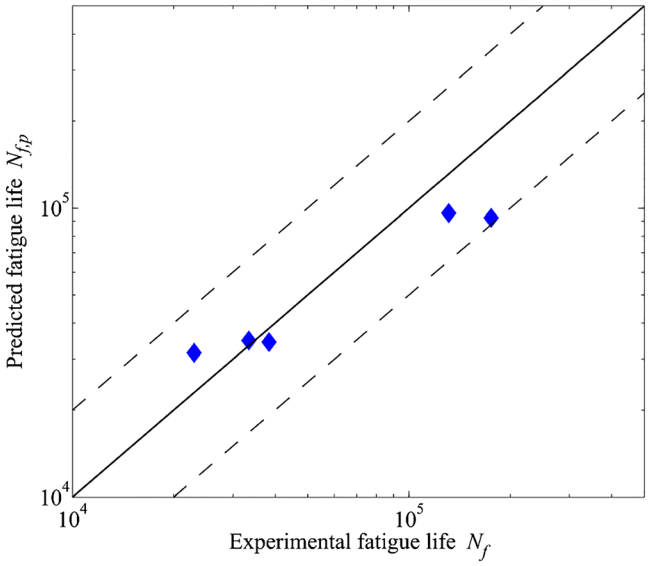

FIGURE 8 Comparison between the predicted fatigue life and the experimental data in Case 2 [Colour figure can be viewed at wileyonlinelibrary.com]

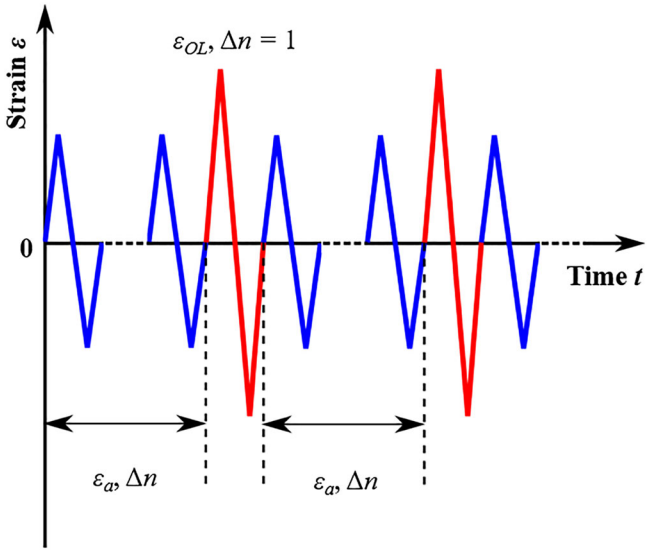

FIGURE 9 Schematic presentation of periodical overloading spectrum of Case 3 [Colour figure can be viewed at wileyonlinelibrary.com]

TABLE 6 Loading conditions of fatigue tests in Case 3[49]

	Stable condition		Overload condition	
Test no.	ε_a (%)	Δn	ε_{OL} (%)	Δn
1	0.3	400	1.0	1
2	0.5	10	1.0	1
3	0.2	5000	0.5	1
4	0.2	50	0.5	1

TABLE 7 Predicted fatigue life and comparison with experimental data in Case 3

Test no.	$N_{f,p}$	N_f
1	78,130	25,823
2	5900	4335
3	133,580	250,050
4	97,220	77,674

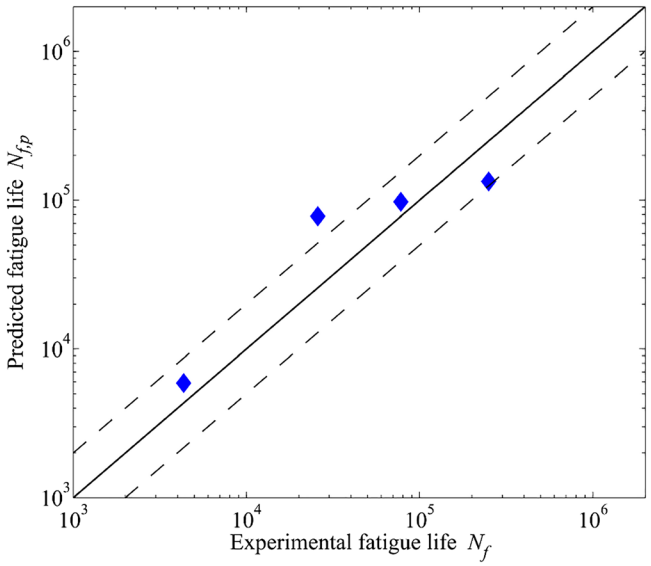

FIGURE 10 Comparison between the predicted fatigue life and the experimental data in Case 3 [Colour figure can be viewed at wileyonlinelibrary.com]

within the specified scatter band, demonstrating therefore the good predication ability of the proposed model for periodical overloading spectrum. The estimated error factor E_S is about 0.288. This is much lower than the E_S given by Miner's rule, which is about 0.502. Hence, it shows that the new QTM-based model developed in this work is superior to Miner's rule in dealing with the effect of overloading on fatigue life.

4 | CONCLUSIONS

This study brings some important improvements on the original QTM approach for fatigue life assessment under VAL. The major improvement focuses on the establishment of a new energy dissipation-based model that is able to consider the nonlinear damage accumulation under VAL. This new model is based on experimental data for the evaluation of the critical energy to failure and applies to both LCF and HCF regimes. It takes into

account the fatigue loading sequence effect that cannot be considered by the traditional cumulative damage model based on Miner's rule.

The proposed model for fatigue life prediction under VAL was applied to three cases of step fatigue tests with different loading sequences, involving two-step loading, repeating two-step loading, and periodical overloading. The values of the fatigue life predicted by the developed QTM are in good agreement with the experimental data. Its prediction accuracy is superior to that of Miner's rule in all the three study cases involved.

Further developments on the QTM are anticipated. The current test cases are relatively simple, involving only two amplitudes of strain; thus, further tests with more load amplitudes are necessary. The adopted fatigue tests were all carried at a fixed loading ratio $R = -1$, so the loading ratio effect was not considered. This needs to be further investigated by considering fatigue loading history with strain levels applied at different loading ratios. Moreover, different types of loading conditions (e.g., torsion and bending) and materials should be investigated.

ACKNOWLEDGMENTS

The authors acknowledge the support from the National Natural Science Foundation of China (No. 51975195), the National Science Fund for Distinguished Young Scholars (No. 51725502), the Special Funds for the Construction of Innovative Provinces in Hunan Province (No. 2019GK4006), and the National Defence Fundamental Research Foundation of China (No. JCKY2020110C105). Open Access Funding provided by Universita degli Studi di Messina within the CRUI-CARE Agreement.

AUTHOR CONTRIBUTIONS

Ensheng Feng: Writing – original draft & editing, Analysis and interpretation of the data, Methodology. **Xiaogang Wang:** Writing – review & comment & editing, Conceptualization, Methodology, Supervision. **Chao Jiang:** Writing – review & comment, Supervision. **Vincenzo Crupi:** Writing – review & editing, Conceptualization, Analysis and interpretation of the data, Methodology, Supervision.

DATA AVAILABILITY STATEMENT

The data that support the findings of this study are not openly available.

NOMENCLATURE

C	specific heat
d_1	intrinsic dissipation
$d_{1,AS}$	asymptotic intrinsic dissipation
$d_{1,\mathrm{cum}}$	total cumulated energy dissipation
D	fatigue damage
D_i	cumulative fatigue damage at the end of the ith block load
E_C	energy tolerance to failure (J m^{-3})
$E_{C,HCF}$	energy tolerance to failure in the high cycle fatigue regime (J m^{-3})
$E_{C,LCF}$	energy tolerance to failure in the low cycle fatigue regime (J m^{-3})
E_d	dissipated energy per cycle (J m^{-3})
$E_{d,i}$	dissipated energy per cycle under the ith block load (J m^{-3})
E_S	error factor
k	thermal conductivity
n_i	cumulative number of cycles at the end of the ith block load
$n_{i-1,e}$	equivalent number of cycles of n_{i-1} corresponding to the ith block load
N_f	fatigue life
$N_{f,p}$	predicted fatigue life
N_r	residual fatigue life
$N_{r,p}$	predicted residual fatigue life
N_t	transition life
q	exponent of the proposed model
$\dot{Q}$	rate of energy dissipated as heat
$\dot{W}$	rate of mechanical work applied to the material
r	external heat source
R	loading ratio
S_{the}	thermoelastic source
t	time
$\dot{U}$	rate of internal energy accumulation in the material
$\dot{U}_D$	internal energy storage rate
$\dot{U}_e$	elastic energy variation rate
β	proportion of dissipated plastic energy
δ	parameter of the proposed model to describe the nonlinear effect
Δn_i	number of cycles of the ith block load
ε_a	strain amplitude
ε_{OL}	overload strain amplitude
ε_{at}	strain amplitude at the transition life N_t
μ	parameter of the proposed model to describe the loading sequence effect
ρ	mass density of material
τ	time constant characterizing the local heat losses
θ_{AS}	asymptotic temperature increment

ORCID

Xiaogang Wang https://orcid.org/0000-0001-7479-8869
Chao Jiang https://orcid.org/0000-0001-5421-9671
Vincenzo Crupi https://orcid.org/0000-0001-7498-4733

REFERENCES

1. Lazzarin P, Tovo R. A notch intensity factor approach to the stress analysis of welds. *Fatigue Fract Eng Mater Struct*. 1998; 21(9):1089-1103.
2. Radaj D. State-of-the-art review on extended stress intensity factor concepts. *Fatigue Fract Eng Mater Struct*. 2014;37(1): 1-28.
3. Ferro P, Berto F, Lazzarin P. Generalized stress intensity factors due to steady and transient thermal loads with applications to welded joints. *Fatigue Fract Eng Mater Struct*. 2006;29(6): 440-453.
4. Lazzarin P, Berto F, Elices M, Gómez J. Brittle failures from U- and V-notches in mode I and mixed, I+ II, mode: a synthesis based on the strain energy density averaged on finite-size volumes. *Fatigue Fract Eng Mater Struct*. 2009;32(8):671-684.
5. Foti P, Berto F. Fatigue assessment of high strength welded joints through the strain energy density method. *Fatigue Fract Eng Mater Struct*. 2020;43(11):2694-2702.
6. Liao D, Zhu SP, Correia JA, de Jesus AM, Berto F. Recent advances on notch effects in metal fatigue: A review. *Fatigue Fract Eng Mater Struct*. 2020;43(4):637-659.
7. Taylor D. *The Theory of Critical Distances: A New Perspective in Fracture Mechanics*. Elsevier; 2007.
8. Crupi V, Guglielmino E, Risitano A, Taylor D. Different methods for fatigue assessment of T welded joints used in ship structures. *J Ship Res*. 2007;51(2):150-159.
9. Taylor D. A mechanistic approach to critical-distance methods in notch fatigue. *Fatigue Fract Eng Mater Struct*. 2001;24(4): 215-224.
10. Saiprasertkit K. Fatigue strength assessment of load-carrying cruciform joints in low-and high-cycle fatigue region based on effective notch strain concept. *Weld World*. 2014;58(4):455-467.
11. Dong P, Pei X, Xing S, Kim MH. A structural strain method for low-cycle fatigue evaluation of welded components. *Int J Press Vessel Pip*. 2014;119:39-51.
12. Pei X, Dong P. An analytically formulated structural strain method for fatigue evaluation of welded components incorporating nonlinear hardening effects. *Fatigue Fract Eng Mater Struct*. 2019;42(1):239-255.
13. Han Q, Wang P, Lu Y. Path-dependent multiaxial fatigue prediction of welded joints using structural strain method. *Fatigue Fract Eng Mater Struct*. 2021;44(10):2800-2826.
14. Zerbst U, Madia M. Fracture mechanics based assessment of the fatigue strength: approach for the determination of the initial crack size. *Fatigue Fract Eng Mater Struct*. 2015;38(9):1066-1075.
15. Dengel D, Harig H. Estimation of the fatigue limit by progressively-increasing load tests. *Fatigue Fract Eng Mater Struct*. 1980;3(2):113-128.
16. Curti G, La Rosa G, Orlando M, Risitano A. Analisi tramite infrarosso termico della temperatura limite in prove di fatica. Proceedings, XIV Convegno Nazionale AIAS. Catania (Italy), 1986:211-220.
17. La Rosa G, Risitano A. Thermographic methodology for rapid determination of the fatigue limit of materials and mechanical components. *Int J Fatigue.* 2000;22(1):65-73.
18. Fargione G, Geraci A, La Rosa G, Risitano A. Rapid determination of the fatigue curve by the thermographic method. *Int J Fatigue.* 2002;24(1):11-19.
19. Amiri M, Khonsari M. Life prediction of metals undergoing fatigue load based on temperature evolution. *Mat Sci Eng a.* 2010;527(6):1555-1559.
20. Fan J, Guo X, Wu C, Crupi V, Guglielmino E. Influence of heat treatments on mechanical behavior of FV520B steel. *Exp Tech*. 2015;39(2):55-64.
21. Curà F, Gallinatti AE, Sesana R. Dissipative aspects in thermographic methods. *Fatigue Fract Eng Mater Struct*. 2012;35(12): 1133-1147.
22. Luong MP. Infrared thermographic scanning of fatigue in metals. *Nucl Eng Des*. 1995;158(2-3):363-376.
23. Luong MP. Fatigue limit evaluation of metals using an infrared thermographic technique. *Mech Mater*. 1998;28(1-4): 155-163.
24. Plekhov O, Saintier N, Palin-Luc T, Uvarov S, Naimark O. Theoretical analysis, infrared and structural investigations of energy dissipation in metals under cyclic loading. *Mat Sci Eng a*. 2007;462(1-2):367-369.
25. De Finis R, Palumbo D, da Silva MM, Galietti U. Is the temperature plateau of a self-heating test a robust parameter to investigate the fatigue limit of steels with thermography? *Fatigue Fract Eng Mater Struct*. 2018;41(4):917-934.
26. Meneghetti G, Ricotta M. Estimating the intrinsic dissipation using the second harmonic of the temperature signal in tension-compression fatigue: Part I. *Theory Fatigue Fract Eng Mater Struct*. 2021;44(8):2168-2185.
27. Teng Z, Wu H, Boller C, Starke P. Thermodynamic entropy as a marker of high-cycle fatigue damage accumulation: example for normalized SAE 1045 steel. *Fatigue Fract Eng Mater Struct*. 2020;43(12):2854-2866.
28. Skibicki D, Lipski A. Evaluation of plastic strain work and multiaxial fatigue life in CuZn37 alloy by means of thermography method and energy-based approaches of Ellyin and Garud. *Fatigue Fract Eng Mater Struct*. 2018;41(12):2541-2556.
29. Maquin F, Pierron F. Heat dissipation measurements in low stress cyclic loading of metallic materials: from internal friction to micro-plasticity. *Mech Mater*. 2009;41(8):928-942.
30. Biot MA. Thermoelasticity and irreversible thermodynamics. *J Appl Phys*. 1956;27(3):240-253.
31. Enke NF. Thermographic stress analysis of isotropic materials. 1990.
32. Ranc N, Wagner D, Paris PC. Study of thermal effects associated with crack propagation during very high cycle fatigue tests. *Acta Mater*. 2008;56(15):4012-4021.
33. Crupi V, Chiofalo G, Guglielmino E. Using infrared thermography in low-cycle fatigue studies of welded joints. *Weld J*. 2010; 89(9):195-200.
34. Wang X, Crupi V, Guo X, Zhao Y. Quantitative thermographic methodology for fatigue assessment and stress measurement. *Int J Fatigue*. 2010;32(12):1970-1976.
35. Wang X, Crupi V, Jiang C, Guglielmino E. Quantitative thermographic methodology for fatigue life assessment in a multiscale energy dissipation framework. *Int J Fatigue.* 2015;81: 249-256.
36. Wang X, Crupi V, Jiang C, Feng E, Guglielmino E, Wang C. Energy-based approach for fatigue life prediction of pure copper. *Int J Fatigue.* 2017;104:243-250.
37. Boulanger T, Chrysochoos A, Mabru C, Galtier A. Calorimetric analysis of dissipative and thermoelastic effects

associated with the fatigue behavior of steels. *Int J Fatigue*. 2004;26(3):221-229.
38. Yang B, Liaw P, Morrison M, et al. Temperature evolution during fatigue damage. *Intermetallics*. 2005;13(3-4):419-428.
39. Yang B, Liaw P, Wang H, et al. Thermographic investigation of the fatigue behavior of reactor pressure vessel steels. *Mat Sci Eng a*. 2001;314(1-2):131-139.
40. Liaw P, Wang H, Jiang L, et al. Thermographic detection of fatigue damage of pressure vessel steels at 1,000 Hz and 20 Hz. *Scripta Mater*. 2000;42(4):389-395.
41. Susmel L. *Multiaxial Notch Fatigue: From Nominal to Local Stress-Strain Quantities*. Woodhead & CRC; 2009.
42. Kueppers M, Sonsino C. Critical plane approach for the assessment of the fatigue behaviour of welded aluminium under multiaxial loading. *Fatigue Fract Eng Mater Struct*. 2003;26(6):507-513.
43. Luo P, Yao W, Susmel L. An improved critical plane and cycle counting method to assess damage under variable amplitude multiaxial fatigue loading. *Fatigue Fract Eng Mater Struct*. 2020;43(9):2024-2039.
44. Feng E, Wang X, Jiang C. A new multiaxial fatigue model for life prediction based on energy dissipation evaluation. *Int J Fatigue*. 2019;122:1-8.
45. Wang X, Ran H, Jiang C, Fang Q. An energy dissipation-based fatigue crack growth model. *Int J Fatigue*. 2018;114:167-176.
46. Palmgren A. Die lebensdauer von kugellargern. *Zeitshrift des Vereines Duetsher Ingenieure*. 1924;68(4):339-410.
47. Miner MA. Cumulative damage in fatigue. *J Appl Mech*. 1945;12(3):A159-A164.
48. Meneghetti G, Ricotta M, Atzori B. Experimental evaluation of fatigue damage in two-stage loading tests based on the energy dissipation. *Proceedings of the Institution of Mechanical Engineers, Part C: J Mech Eng Sci*. 2015;229(7):1280-1291.
49. Kamaya M, Kawakubo M. Loading sequence effect on fatigue life of Type 316 stainless steel. *Int J Fatigue*. 2015;81:10-20.
50. Marco S, Starkey W. A concept of fatigue damage. *Trans ASME*. 1954;76(4):627-632.
51. Corten H, Dolan T. Cumulative fatigue damage. Paper presented at: Proceedings of the international conference on fatigue of metals. 1956;235-246.
52. Langer B. Fatigue failure from stress cycles of varying amplitude. *J Appl Mech-T ASME*. 1937;59(4):160-162.
53. Wheeler OE. Spectrum loading and crack growth. *J Basic Eng-T ASME*. 1972;94(1):181-186.
54. El Haddad M, Smith K, Topper T. Fatigue crack propagation of short cracks. *J Eng Mater-T ASME*. 1979;101(1):42-46.
55. Golos K, Ellyin F. A total strain energy density theory for cumulative fatigue damage. *J Press Vess-T ASME*. 1988;110(1):36-41.
56. Fatemi A, Yang L. Cumulative fatigue damage and life prediction theories: a survey of the state of the art for homogeneous materials. *Int J Fatigue*. 1998;20(1):9-34.
57. Jinescu VV. Critical energy approach for the fatigue life calculation under blocks with different normal stresses amplitudes. *Int J Mech Sci*. 2013;67:78-88.
58. Chrysochoos A, Louche H. An infrared image processing to analyse the calorific effects accompanying strain localisation. *Int J Eng Sci*. 2000;38(16):1759-1788.
59. Giancane S, Chrysochoos A, Dattoma V, Wattrisse B. Deformation and dissipated energies for high cycle fatigue of 2024-T3 aluminium alloy. *Theor Appl Fract Mec*. 2009;52(2):117-121.
60. Bever MB, Holt DL, Titchener AL. The stored energy of cold work. *Prog Mater Sci*. 1973;17:5-177.
61. Fan J, Zhao Y, Guo X. A unifying energy approach for high cycle fatigue behavior evaluation. *Mech Mater*. 2018;120:15-25.
62. Teng Z, Wu H, Boller C, Starke P. A unified fatigue life calculation based on intrinsic thermal dissipation and microplasticity evolution. *Int J Fatigue*. 2020;131:105370.
63. Rosakis P, Rosakis AJ, Ravichandran G, Hodowany J. A thermodynamic internal variable model for the partition of plastic work into heat and stored energy in metals. *J Mech Phys Solids*. 2000;48(3):581-607.
64. Wang X, Feng E, Jiang C. A microplasticity evaluation method in very high cycle fatigue. *Int J Fatigue*. 2017;94:6-15.
65. Guo Q, Guo X, Fan J, Syed R, Wu C. An energy method for rapid evaluation of high-cycle fatigue parameters based on intrinsic dissipation. *Int J Fatigue*. 2015;80:136-144.
66. Teng Z, Wu H, Boller C, Starke P. Thermography in high cycle fatigue short-term evaluation procedures applied to a medium carbon steel. *Fatigue Fract Eng Mate Struct*. 2020;43(3):515-526.
67. Lemaitre J, Plumtree A. Application of damage concepts to predict creep-fatigue failures. *J Eng Mater Technol*. 1979;101(3):284-292.
68. Aeran A, Vantadori S, Carpinteri A, Siriwardane SC, Scorza D. Novel non-linear relationship to evaluate the critical plane orientation. *Int J Fatigue*. 2019;124:537-543.
69. Jang J, Khonsari MM. On the prediction of fatigue life subjected to variable loading sequence. *Fatigue Fract Eng Mater Struct*. 2021;44(11):2962-2974.
70. Ueno H, Kakihata K, Kaneko Y, Hashimoto S, Vinogradov A. Enhanced fatigue properties of nanostructured austenitic SUS 316L stainless steel. *Acta Mater*. 2011;59(18):7060-7069.
71. Kawakubo M, Kamaya M. Fatigue life prediction of stainless steel under variable loading (damage factors determining fatigue life and damage evaluation for two-step test). *Journal of the Society of Materials Science, Japan*. 2011;60(10):871-878.
72. Slot H, Matthews D, Schipper D, van der Heide E. Fatigue-based model for the droplet impingement erosion incubation period of metallic surfaces. *Fatigue Fract Eng Mater Struct*. 2021;44(1):199-211.
73. Park J, Nelson D. Evaluation of an energy-based approach and a critical plane approach for predicting constant amplitude multiaxial fatigue life. *Int J Fatigue*. 2000;22(1):23-39.

How to cite this article: Feng E, Wang X, Jiang C, Crupi V. Quantitative thermographic method for fatigue life prediction under variable amplitude loading. *Fatigue Fract Eng Mater Struct*. 2022;45(4):1199-1212. doi:10.1111/ffe.13658